ASSESSING THE IMPACT OF SEA LEVEL RISE ON PORT OPERABILITY USING LIDAR-DERIVED DIGITAL ELEVATION MODELS

Vicente Gracia[1,2]
Joan Pau Sierra[1,2]
Marta Gómez[3]
Mónica Pedrol[3]
Sara Sampé[3]
Manuel García-León[2]
Xavier Gironella[1,2]

[1]Laboratori d'Enginyeria Marítima, Universitat Politècnica de Catalunya BarcelonaTech, Jordi Girona 1-3, Mòdul D1, Campus Nord, 08034 Barcelona, Catalonia, Spain

[2]Centre Internacional d'Investigació dels Recursos Costaners (CIIRC), Jordi Girona 1-3, Mòdul D1, Campus Nord, 08034 Barcelona, Catalonia, Spain

[3]Departament d'Enginyeria Civil i Ambiental, Universitat Politècnica de Catalunya BarcelonaTech, Jordi Girona 1-3, Campus Nord, 08034 Barcelona, Catalonia, Spain

Corresponding author: Vicente Gracia, e-mail: vicente.gracia@upc.edu, Telephone: +34 934017391, Fax: +34934011861, ORCID id: orcid.org/0000-0002-4628-426X

Abstract

One of the main consequences of climate change is the sea level rise (SLR), which impacts coastal areas affecting many infrastructures, particularly seaports, whose operations may be jeopardized. In this paper, a methodological framework is developed to assess the impact of SLR on port operability by using digital elevation models derived from LiDAR data. The methodology is applied to four ports along the Catalan Coast (NW Mediterranean). The study is made for the RCP8.5 scenario from IPCC, analysing port operability every 10 years throughout the 21st century. The approach provided here allows a port authority to determine which berthing areas will be affected at each port and at each time interval. Results show that, if no adaptation measures are taken, ports will have significant reductions of present operability for most of their activities, in particular after year 2070. This work shows that the developed methodological framework is a very useful tool for port authorities to detect operability tipping points and to design well in advance the necessary adaptation pathways to overcome the expected impacts.

Keywords: Port operability, Sea level rise, LiDAR, RCP8.5 scenario, DEM.

1. INTRODUCTION

Coastal areas are among the systems most vulnerable to climate change due to sea level rise (SLR). Among other effects, SLR will directly flood large coastal stretches and will change the littoral processes as for example the sediment transport patterns (Nicholls et al., 2011; Sánchez-Arcilla et al., 2011).

Many studies have analysed the impacts of SLR on beaches (Stive, 2004; Torresan et al., 2012; Paudel et al. 2015; Monioudi et al., 2016), flooding of coastal areas (Brown, 2006; Revell et al., 2011; Le Cozannet et al., 2015), coastal habitats (Chu-Agor et al., 2011; Kane et al., 2015; Clough et al., 2016), coastal defence structures (Chini and Stansby, 2012; Isobe, 2013; Burchart et al., 2014) or the flooding of coastal urban areas (Hallegate et al., 2011; Paudel et al., 2015).

Since seaports are located on the coast or in estuaries they will also be affected by SLR (Sánchez-Arcilla et al., 2016; Sierra et al., 2017a). Nevertheless, the studies addressing the impacts of climate change on ports (Becker et al., 2012; Masse et al., 2013; Ng et al., 2013; Suh et al., 2013; Sánchez-Arcilla et al., 2016; Sierra et al., 2016, 2017a) are few compared with the numerous analyses carried out in coastal areas (Sierra et al., 2017b).

One of the main potential impacts of SLR on ports is the loss of operability due to reduction of freeboard in the berthing areas or even the dock flooding (Sánchez-Arcilla et al., 2016). In addition, SLR will increase the water depth around and inside the harbour. These new water depths will change the present wave propagation patterns (shoaling, refraction and diffraction processes). This can in turn produce additional impacts on ports like changes in agitation, siltation or structure stability (Sierra and Casas-Prat, 2014). The impacts may be either positive or negative, i.e. they can improve or worsen port operability (Sierra et al., 2016).

To study potential impacts of SLR on coastal areas, accurate topographic information is needed. In order to extract this information, Digital Elevation Models (DEMs) are commonly used due to their availability and relatively low cost (or even free access) when obtained from governmental sources (Yamamoto et al., 2012). Frequently, these DEMs are constructed from remotely sensed data. LiDAR (Light Detection and Ranging) data has become a very common source of information from which DEMs may be obtained with multiple applications to geosciences (Goulden et al., 2016). Thus, for example, LiDAR-derived DEMs have been used for measuring the 3D structure of forests (Wulder et al., 2012), for assessing forest biomass (Knapp et al., 2018), for urban land cover classification (Brennan and Webster, 2006; Chehata et al., 2009; Alexander et al., 2010; Guo et al., 2011; Zhou, 2013) and in hydrological studies (Goulden et al., 2014, 2016 among others).

In the last years, LiDAR-derived DEMs have also been successfully used for oceanic and coastal investigations: characterization of tidal marshes (Hladik and Alber, 2012; Buffington et al., 2016); measurement of shoreline changes (Revell et al., 2002; White and Wang, 2003; Shrestha et al., 2005; Addo et al., 2008); identification of low-lying areas prone to be inundated (Straatsma and Middelkoop, 2006); management of coastal defences (Pe'eri and Long, 2011); mapping of dunes for coastal protection (Stockton et al., 2009; Richter et al., 2013); visualization of bathymetric features for habitat identification (Collin et al., 2008; Yamamoto et al., 2012); definition of topographic complexity of coral reefs (Costa et al., 2009; Zawada and Brock, 2009); and measurement of particle distributions of the upper ocean (Hill et al., 2013; Behrenfeld et al., 2017; Collister et al., 2018).

A number of studies have focussed on the assessment of SLR impacts on coastal areas using LiDAR-derived DEMs (Webster et al., 2006; Poulter and Halpin, 2008; Gesh, 2009; Wu et al., 2009; Zhang, 2011; Cooper et al., 2013) but, as far as the authors know, there are no studies using this technique to analyse the potential impacts of sea-level rise on ports. Nevertheless, LiDAR-based DEMs could be very useful to study such impacts, in particular the loss of terminal operability and the dock flooding.

Therefore, the objective of this paper is to develop a methodological framework using LiDAR-derived DEMs that can be used to assess changes in port operability due to SLR. This framework will be then applied to four ports of the Catalan Coast (NW Mediterranean), in which fishing, leisure and even commercial activities are carried out to illustrate its potential as a useful tool for future port planning oriented to adaptation to SLR.

The paper is structured as follows: in Section 2, the different parts of the methodological framework are widely described. In Section 3, the application of the methodology to the ports is presented, while in Section 4 the results are discussed. Finally, in Section 5 the main conclusions of the work are summarized.

2. METHODS

Sea level rise (SLR) induced by global warming will affect present port operability by reducing the existing freeboard in docks and piers. The extent to which climate change will affect a specific port operation depends on the features of such port operation. Container ships or general cargo vessels, due to their dimensions, require the largest freeboards whereas leisure boats, located in the shallower areas of the harbour due to their reduced draught, have the smallest freeboard needs. Another aspect to be considered is the elevation reached by the infrastructure. An accurate definition of the geometry of piers and docks is necessary to determine precisely how a specific rise of the mean water level will affect port operability.

The methodology used to assess the degree of impact on services due to SLR for a specific harbour follows 4 main steps: (i) the building of the port Digital Elevation Model (DEM); (ii) the identification of the areas of interest and their characteristics in terms of type of structure and port operation; (iii) the time variability of the mean water level for present conditions and under a climate change scenario and (iv) the construction of port operability maps for different time frames.

2.1. DEM building

As indicated in Section 1, the high resolution digital geospatial information derived from LiDAR makes it particularly useful in many fields of geosciences. In this study a DEM has been constructed for each considered port from LiDAR and topographic data freely available at the Institut Cartogràfic i Geològic de Catalunya (ICGC), which is the government agency that has the competences on geodesy, cartography and geographic information, at regional level. Both types of data were downloaded from the web page (http://www.icc.cat/vissir3/) of this institute.

LiDAR data collection in the four areas of interest was carried out in flights made in 2010, between April and July. The cloud of Airborne Light Scanning points was captured with a LiDAR sensor (Leica ALS50-II) and calibrated and adjusted with topographic control points. The altimetry accuracy has a Root Mean Square Error (RMSE) of about 6 cm for flat low vegetated areas as it is the case of harbours. The point density ranges between 0.5 and 0.7 points/m^2, and they are automatically classified according to the American Society for Photogrammetry and Remote Sensing (ASPRS) standards. Data are available in square areas of 2 x 2 Km. Table 1 lists the LiDAR files downloaded from the ICGC webpage and used in this work, as well as some of their features.

Table 1. LiDAR files downloaded from the ICGC webpage. Coordinates (UTM, fuse 31, ETRS89) are those corresponding to the SW vertex of each 2 x 2 Km area.

Area	**File name (.las)**	**x coordinate**	**Y coordinate**	**Density (points/m^2)**	**Flight date**
Palamós	lidarcatv01ls12f508632ed01	508000	4632000	0.5	June 2010
Arenys Mar	lidarcatv01ls12f462602ed01	462000	4602000	0.5	July 2010
Vilanova G.	lidarcatv01ls12f392562ed01	392000	4562000	0.7	May 2010
Vilanova G.	lidarcatv01ls12f394562ed01	394000	4562000	0.7	May 2010
Cambrils	lidarcatv01ls12f336546ed01	336000	4546000	0.7	April 2010

Topographic information from ICGC at 1/5,000 and 1/1,000 scales is combined with the LAS data set in each port to construct its DEM. This information was obtained from photogrammetric flights carried out between 2009 and 2013 using a digital camera of Z-Imaging type (Leica ADS40). The accuracy of the topographic cartography is 20 cm in planimetry and 25 cm in altimetry with contour lines every 1 m. All data coordinates are projected in UTM fuse 31 and the geodesic reference system considered is ETRS89. Orthometric altitudes are referred to the EGM08D595 geoid. The original EPSG is 25831 and the supported OGCs are WMS 1.0.0, 1.1.0, 1.1.1, 1.3.0. The Geographic Information System (GIS) ArcMap® is used to manage all the information and analyse the port operability. In Table 2, the files used in this work and downloaded from the ICGC webpage are included.

Table 2. Topographic files downloaded from the ICGC webpage.

Area	File name (.shp)	Data type	Scale
Palamós	ct1mv22sh0a001844054400axn1r010	Points with elevation	1:1000
Palamós	ct1mv22sh0a001844054400axl1r010	Lines	1:1000
Arenys de Mar	bt5mv20sh0f298117an1r040	Points with elevation	1:5000
Arenys de Mar	bt5mv20sh0f299117an1r040	Points with elevation	1:5000
Arenys de Mar	bt5mv20sh0f298117al1r040	Lines	1:5000
Arenys de Mar	bt5mv20sh0f299117al1r040	Lines	1:5000
Vilanova I la Geltrú	ct1mv22sh0f001844055000axn1r010	Points with elevation	1:1000
Vilanova I la Geltrú	ct1mv22sh0f001844055000axl1r010	Lines	1:1000
Cambrils	ct1mv22sh0f001755006500axn1r010	Points with elevation	1:1000
Cambrils	ct1mv22sh0f001755006500axl1r010	Lines	1:1000

The complete procedure is as follows (see flowchart in Figure 1). The LiDAR dataset is downloaded in LAZ format, a compact data file. To visualize this data using GIS, the files must be uncompressed obtaining the data in LAS 1.2 format (Figure 2b), and a LAS dataset must be created using ArcCatalog®. The uncompressing LiDAR data process from LAZ to LAS format is carried out without information loss. Using ArcMap® the point cloud is converted into vector data, that is, a multipoint shapefile. The type of points to be converted from the cloud of LAS points must be specified according to the ASPRS standard. In this procedure it is important to properly define

the point density of the LiDAR data file in order to obtain admissible models adjusted to the reality. In addition, the study area or area of interest (AOI) is delimited by creating a polygon shapefile, which combined with the multipoint LAS and the Topographic and Cartographic (TC) shapefiles (Figure 2a), gives rise to two shapefiles for the AOI. By merging the information of both files, a Triangular Irregular Network (TIN) file is created (Figure 2c). ArcMap® 3D tool is used for this step and it considers the points as spot locations of elevation data and the lines to enforce natural features. In the TIN creation process, the role of each data source input and how they have to be used in the TIN must be established. The feature types that can be used to build the TIN surface are mass points, breaklines and hulls, and polygons. The mass points are point height measurements; they become nodes in the TIN network and determine the overall shape of the surface. Breaklines and hulls are lines with or without height measurements. They become sequences of one or more triangle edges. Breaklines typically represent either natural features, such as ridgelines or streams, or built features, such as roadways. Finally, the polygon feature can be used as four different polygon surface types: clip polygon, erase polygon, replace polygon and fill polygon. The first is the one used in the current case of study. It is the responsible of defining the boundary for the TIN surface. Finally, a DEM (Figure 2d) is generated from the TIN using linear interpolation. The sampling distance of the output raster is determined as a 0.5 m x 0.5 m cell sized DEM, since the minimum density of point cloud used is 0.5 points/m^2 as mentioned before, and therefore, there is enough information to obtain a raster of this resolution. Moreover, a float data type for the output raster has been considered, which uses 32-bit floating point, supporting values ranging from -3.402823466e+38 to 3.402823466e38. Figure 1 summarizes the followed steps for the construction of the DEM in each studied port, while Figure 2 shows some of the images (corresponding to the different types of data) obtained during the process.

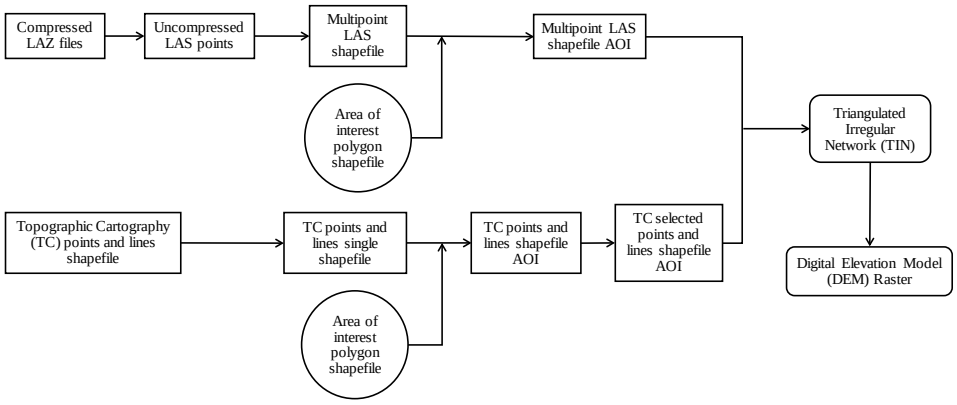

Figure 1. Flowchart of the construction of a DEM of a port. Area of Interest refers to a polygon created reflecting a specific port extension, its port use, the type of infrastructure and the water body.

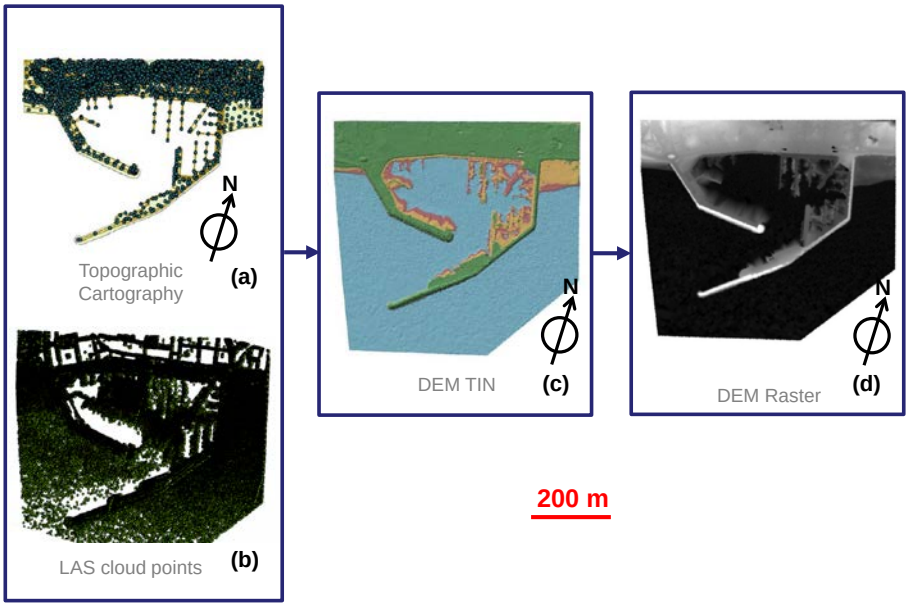

175

176 Figure 2. Data sets, TIN and DEM obtained for the harbour of Cambrils (Catalonia, Spain).

177 **2.2. Present port uses, infrastructures and operability requirements**

178 There are a number of processes that can hinder or even prevent port operations. The main
179 processes that may have such impact on those operations are wind, currents, waves and water
180 levels. If wind or current velocities or wave heights exceed certain thresholds within the harbour
181 and, in particular, nearby docks and piers, operations such as berthing manoeuvres and loading or
182 unloading of goods cannot be carried out safely and most of the times have to be suspended. This
183 leads the affected area to a condition of inoperability.

184 Concerning water levels, a port activity can be performed safely (guarantying the vessel integrity
185 and the port operation) if the distance between the top of the berth and the water level, the
186 freeboard, stays within certain limits. These values can be expressed as a function of the vessel
187 geometry or the port activity. For the sake of simplicity, as the vessels which can operate in a port
188 are too heterogeneous to be considered individually, the requirements referring to the port use

have been taken into account. Because of that, a map of port services and infrastructure use has been defined for each analysed port following the Master Plan of the Catalan Ports (DPTOP, 2007). Fishing, leisure and commercial uses have been identified as the main port activities, and the infrastructure typology giving service to such uses has been categorised in piers and docks.

The safety requirements for the three port activities are taken from the Recommendations for the Design of Maritime Works ROM 2.0-11 (EPPE, 2012), published by the Spanish Port Authority (Puertos del Estado). These recommendations seek to ensure safety and execution of the port operations by determining the minimum freeboard of docks and piers necessary for berthing, mooring and loading/unloading cargo and/or passengers. Although not mandatory, port authorities in Spain have to meet the proposed values to guarantee the different port operations. Table 3 summarizes the port operability requirements taken into account in this case study.

Table 3. Port operability requirements derived from ROM 2.0-11 (EPPE, 2012)

	Commercial use	**Fishery use**	**Leisure use**
Maximum freeboard (m)	2.5	1.0	1.0
Minimum freeboard (m)	1.5	0.5	0.15

A polygon is created for each AOI in which a port activity is observed and the different attributes (type of infrastructure and port use or water body) are assigned to monitor the impact of SLR on it.

2.3. Mean water level oscillations

The mean water level at any instant (t) can be understood as the sum of the astronomical tide component, the storm surge and the SLR induced by global warming.

The astronomical tide reflects the gravitational effects of stars and planets over a specific water body. Water levels due to this forcing can be accurately predicted anytime at any point. High tides

210 can take place once or twice a day depending on the geographic location and due to their
211 permanent nature (although intermittent) they must be considered. The storm surge is the result of
212 the action of a low pressure system and the wind over the sea free surface and is decoupled from
213 astronomical tides. Its effects, although predictable (with less accuracy than tides), usually take
214 place in shorter periods (typically hours) and they are only significant in the case of severe storms,
215 which take place a few times per year. For this reason and its temporary short-lived nature, this
216 component has not been considered in the analysis.

217 The potential impact of SLR induced by climate change on port operability has been done by
218 considering the Representative Concentration Pathway RCP8.5 scenario and its corresponding
219 SLR projection, given in the 5th Assessment Report (AR5) of the IPCC for the Mediterranean Sea
220 (IPCC, 2013). The RCP8.5 corresponds to very high greenhouse gas emissions and for the
221 Mediterranean it is considered to be the 90% of the global value (Sierra et al., 2017b). This is
222 because sea level is expected to decrease in semienclosed and inland seas (e.g. Mediterranean
223 Sea or Black Sea) due to the increase in excess of evaporation (Yin et al., 2010). Therefore,
224 considering the estimations of Vousdoukas et al. (2018) a SLR 10% smaller than the global
225 averages has been considered.

226 Hence, the upper band in year 2100 gives an estimation of SLR of 0.88 m, with respect to the
227 mean water level in 2000. In Figure 3, the projected SLR for RCP8.5 in the Mediterranean Sea
228 until year 2100 is presented, where the 95% confidence bands are also plotted (lower and upper
229 limits). The dataset represented is from 2005 to 2100 and the evidence of the increasing impact of
230 climate change on SLR in the worst scenario can be observed, assuming that no mitigation action
231 is carried out. Although the developed methodology can be applied to any scenario, in this study
232 the values corresponding to the upper band of SLR for RCP8.5 (Table 4) have been selected to
233 assess the impacts for the worst condition projected in AR5.

234 Table 4. Values of SLR (with respect to year 2000) considered in this study (upper bound). In brackets lower
235 bound and central estimate. Elaborated based on Vousdoukas et al. (2018)

Year	SLR (m)
2020	0.11 (0.05, 0.08)
2030	0.17 (0.08, 0.13)
2040	0.24 (0.10, 0.17)
2050	0.33 (0.17, 0.25)
2060	0.42 (0.20, 0.31)
2070	0.52 (0.25, 0.38)
2080	0.63 (0.31, 0.47)
2090	0.75 (0.37, 0.56)
2100	0.88 (0.41, 0.64)

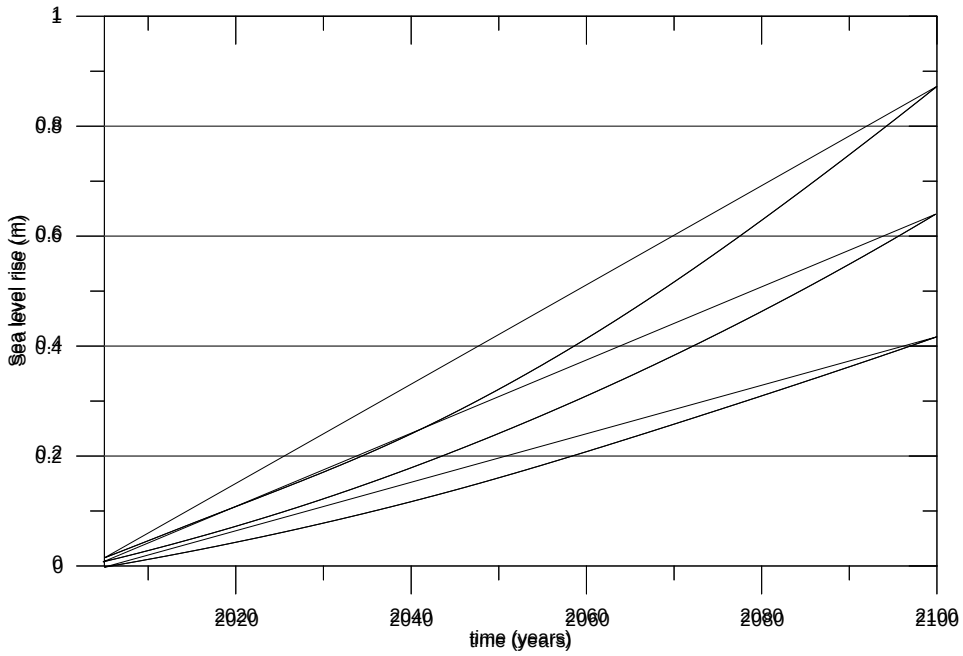

Figure 3. Upper, mean and lower limit of SLR projection for the Mediterranean Sea under the RCP8.5 scenario with respect to year 2000.

2.4. Port operability maps

Once the DEM of the port has been created and the harbour activities are identified the next step is to analyse the effect of SLR on port operability. The analysis is performed every 10 years. This selected time window is large enough to describe a significant variation in SLR and short enough to detect possible tipping points in port operability.

The Reclassify tool in ArcMap® has been used to give new values to the raster's properties according to the selected freeboard criterion. The reclassification is especially useful in this study since it allows to associate an operability level to a given freeboard. Each cell represents 0.5 m x 0.5 m, to which corresponds a certain level of the terrain in the AOI defined in the raster attributes. Therefore, the raster map has been re-classified according to four cases of operability: Maximum operability, minimum operability, not operable and flooded (Figure 4 and Table 5). This process is repeated for each 10 years' time window to determine the time sequence of port operability impacts due to SLR. To do this, a variable MWL is defined as the sum of the mean water level, the mean high astronomical tide and the SLR.

Table 5. Operability status for a specific time interval used in the Reclassify tool in ArcMap®. MWL is the mean water level including the astronomical tide and the SLR due to global warming.

Operability status	Elevation value in DEM raster
Maximum operability	MWL + maximum freeboard
Minimum operability	MWL + minimum freeboard
Not operable	MWL
Flooded	< MWL

The Maximum operability status describes a condition in which the berth's top is located at a level greater or equal than the MWL (represented by the blue line) plus the maximum freeboard

permitted for each port operation, as shown by the green line in Figure 4a. The Minimum operability is achieved when the berth's top matches the MWL plus the minimum freeboard permitted, as indicated by the red line in Figure 4b. The port activity is considered not possible when the berth's top is lower than the MWL plus the minimum freeboard permitted (not operable), as can be seen in Figure 4c where the red line indicating the minimum freeboard necessary has a level greater than the dock's top. Finally, the Flooded situation is reached when the berth's top has a level lower than the MWL (blue line in Figure 4d).

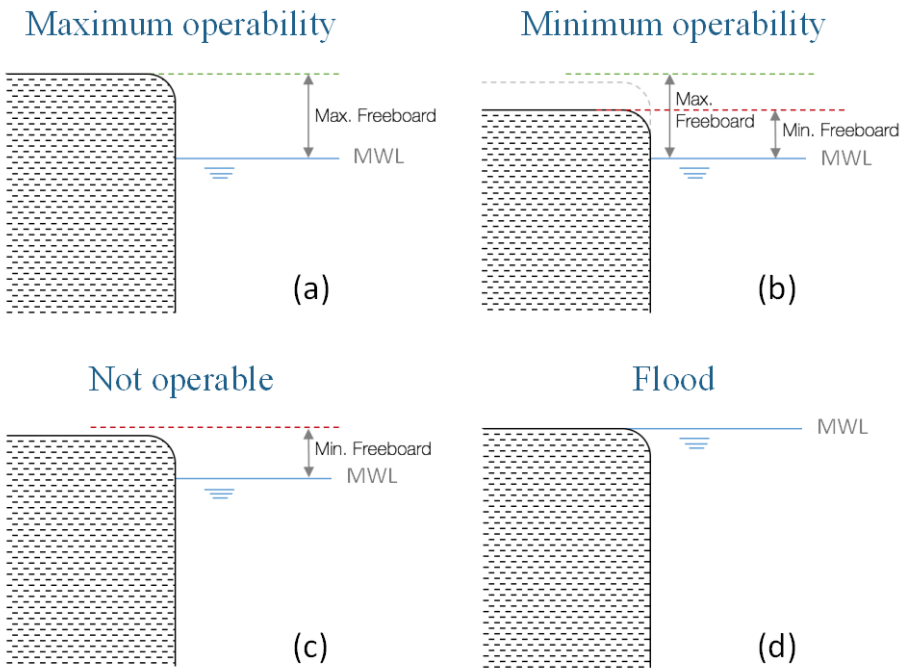

Figure 4. Port operability categories. (a): Maximum operability indicates that the berth's top is located at a level greater or equal than the MWL (blue line) plus the maximum freeboard (green line). (b): Minimum operability is when the berth's top is equal to the MWL plus the minimum freeboard (red line). (c): Not

operable is when the berths top is lower than the MWL plus the minimum freeboard. (d): The berth is flooded when the berth's top has a level lower than the MWL

3. APPLICATION TO THE CATALAN COAST

3.1. Study area

The Catalan coast is located in the NW Mediterranean and it has a length of about 700 km. The area is in a fetch-limited micro-tidal environment, with a tidal range of about 25 cm (Bolaños et al., 2009). There are 47 seaports: 5 commercial harbours (2 large and 3 of medium size) which offer services for fishing and leisure activities as well, 2 industrial ports dedicated to cement, 18 mixed-type ports (fishing and leisure) and 22 marinas.

For this study four ports have been selected trying to characterize the Catalan port system in all their singularities. The main criterion considered has been to cover all type of uses, commercial, fishing and leisure. In addition, the selected port facilities have to be potentially affected in their operability by SLR, they have to be of economic relevance in the region and must be well geographically distributed. Small marinas are not taken into account in the analysis due to their reduced impact in the economic system and also because they typically present flexible infrastructures such as floating piers, that can be moved more easily in time to accommodate new market or environmental demands.

The selected ports are: Palamós, Vilanova i la Geltrú, Arenys de Mar and Cambrils. All of them have fishing and leisure activities and the two first have also a commercial function (loading and unloading of goods and/or passengers). They can be considered as a good representation of the domestic and international sea transport and also are a key element in the short sea shipping. Their main features are summarized in Table 6 and their location and layouts are shown in Figure 5.

298 Table 6. Main features of the 4 studied ports. S_T and S_L are respectively the total port surface and the land
299 surface, both in hectares; L is the berthing length; d is the water depth at the port mouth; Activities are: C
300 (commercial), F (fishing) and L (leisure).

Port	**Longitude**	**Latitude**	**S_T** (ha)	**S_L** (ha)	**L** (m)	**d** (m)	**Activities**
Palamós	3º 07' E	41º 50' N	43.45	18.66	1549	21	CFL
Arenys de Mar	2º 33' E	41º 34' N	29.14	11.77	2314	6	FL
Vilanova i la G.	1º 43' E	41º 12' N	67.22	21.03	3012	7	CFL
Cambrils	1º 03' E	41º 03' N	25.17	8.04	1482	6.5	FL

301
302
303
304
305
306

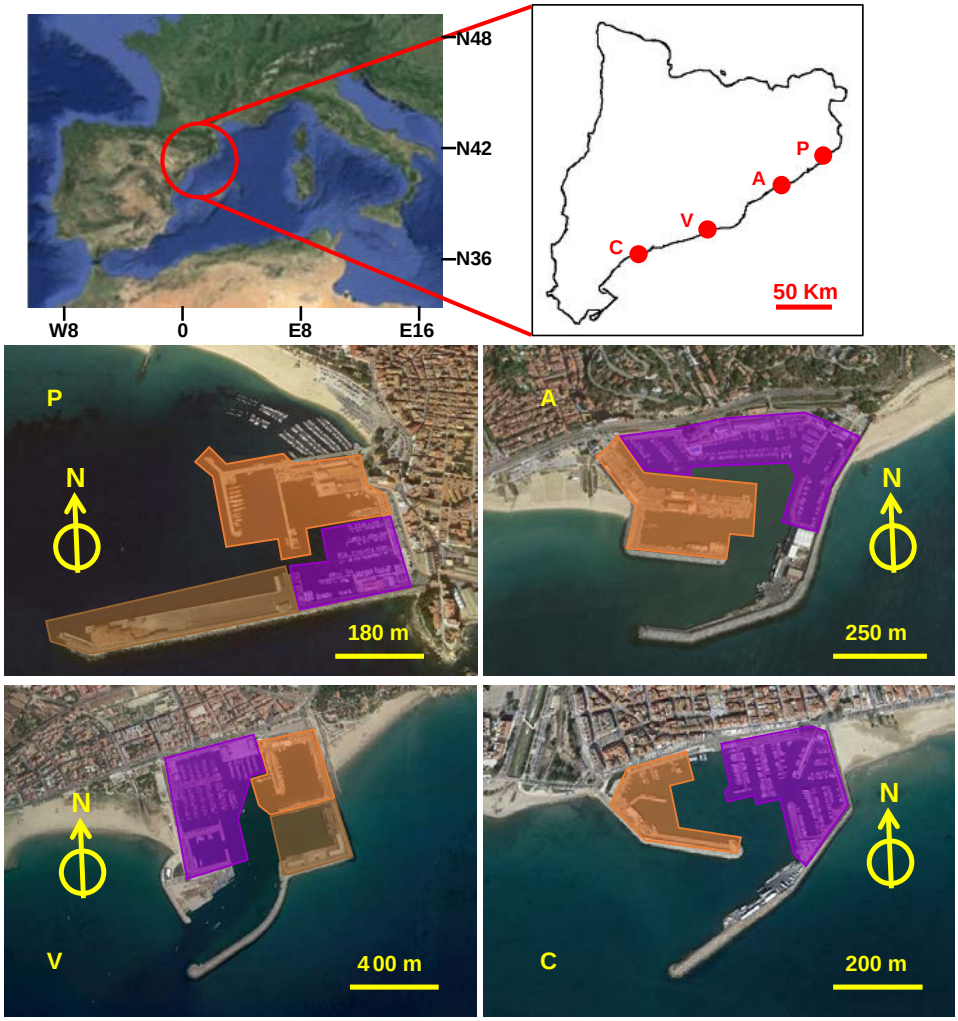

Figure 5. Location of the 4 studied ports and view of their layouts. P: Palamós, A: Arenys de Mar, V: Vilanova i la Geltrú, C: Cambrils. Graphical scales have been added to give an idea of their dimensions. Coloured areas indicate port use: commercial (dark brown), leisure (purple) and fishing (orange). Non-coloured areas correspond to other uses (e.g. dry docks) not analysed.

3.2 Results

In this section the results corresponding to the impact of SLR on the four studied ports are presented, by showing their operability maps. These maps have been built by comparing the resulting freeboard with respect MWL at each considered time (every 10 years) and the values given in Tables 3 and 5. For the sake of simplicity, the freeboards corresponding to each use have been taken into account and mapped in the whole port. Nevertheless, when analysing the operability, only those berthing areas corresponding to each typology (docks or piers) have been considered, accounting the length of the berths affected and computing the percentage that they represent with respect to the total berthing length of its typology. The maps have been plotted and the corresponding operability percentages have been assessed for year 2015 (present situation) and between 2030 and 2100 at 10-year intervals. The time sequence represents the operability evolution at each port during the 21st century. As a sample, in Figures 6 to 9 these maps are presented, corresponding to each port and use for three instants: 2015 (present situation), 2060 (by the middle of the studied period) and 2100 (end of the analysed period).

The presented results have been obtained assuming that no adaptation measures are undertaken by port authorities and, as a consequence, the port morphology is the same during the entire century. In the discussion section, the implications of this hypothesis are analysed. The results show a general reduction of operability in all ports during the 21st century due to SLR. The degree of impact is different depending on the geometric characteristics of the infrastructure. The difference of results in each port is a consequence of their different morphology, in particular the freeboard of the docks. Since even within the same port, various docks can have different freeboard, the impact in each port and for each use is different.

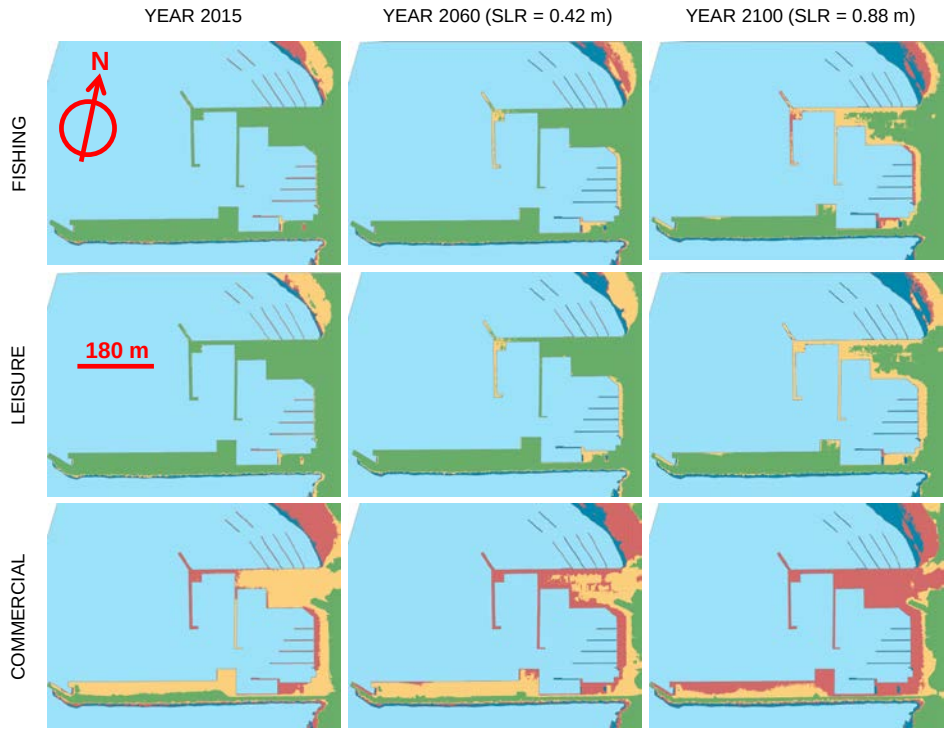

Figure 6. Operability maps of Palamós port in year 2015, 2060 and 2100 for the different port uses. Coloured areas indicate the port operability status: Maximum (green), minimum (light brown), not operable (red) and flooded (blue).

In the case of Palamós (Figure 6) the fishing and leisure berths are fully operative during almost the entire studied period. Only by the end of the century some berths become inoperative. In this port, some commercial berths start to be inoperative by the middle of the century, while in 2100 all this area is inoperative.

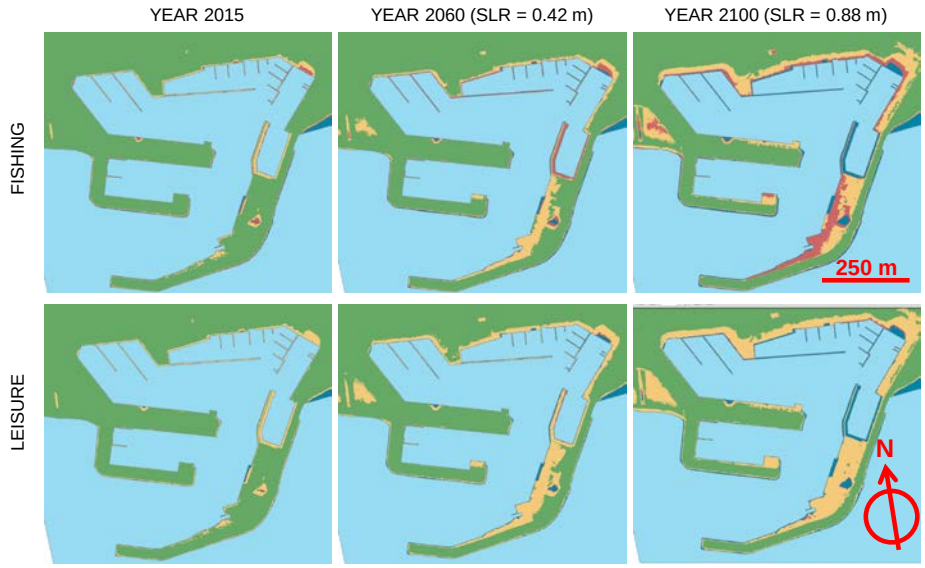

Figure 7. Operability maps of Arenys de Mar port in year 2015, 2060 and 2100 for the different port uses. Coloured areas indicate the port operability status: Maximum (green), minimum (light brown), not operable (red) and flooded (blue).

In Figure 7, the operability evolution for Arenys de Mar port is plotted for fishing and leisure berths (this port has no commercial function). In the fishing sector, a few berths do not meet the operability regulations during all the studied period, being flooded from the middle of the century onwards. In the case of leisure berths, they are all operative at the beginning and middle of the century, but by the end most of them are flooded.

The maps corresponding to the fishing and leisure services for Vilanova i la Geltrú port are shown in Figure 8. In the fishing zone, some berths start to be inoperative by the middle of the century, while by its end most of them are inoperative. In the same way, leisure berths follow a similar pattern. The main difference is that by the end of the century most of these leisure berths are not only inoperative but even flooded.

Finally, Figure 9 shows the operability evolution maps for Cambrils port and its two functions, fishing and leisure. For the fishing function, some berths have a freeboard under the recommended operability threshold for this type of boats, which become flooded by the middle of the century. In 2100 all these berths would be inoperative for this SLR scenario, although only few additional berths would be flooded. In the case of leisure boats, the number of berths inoperative would be small by 2060, increasing very much by 2100.

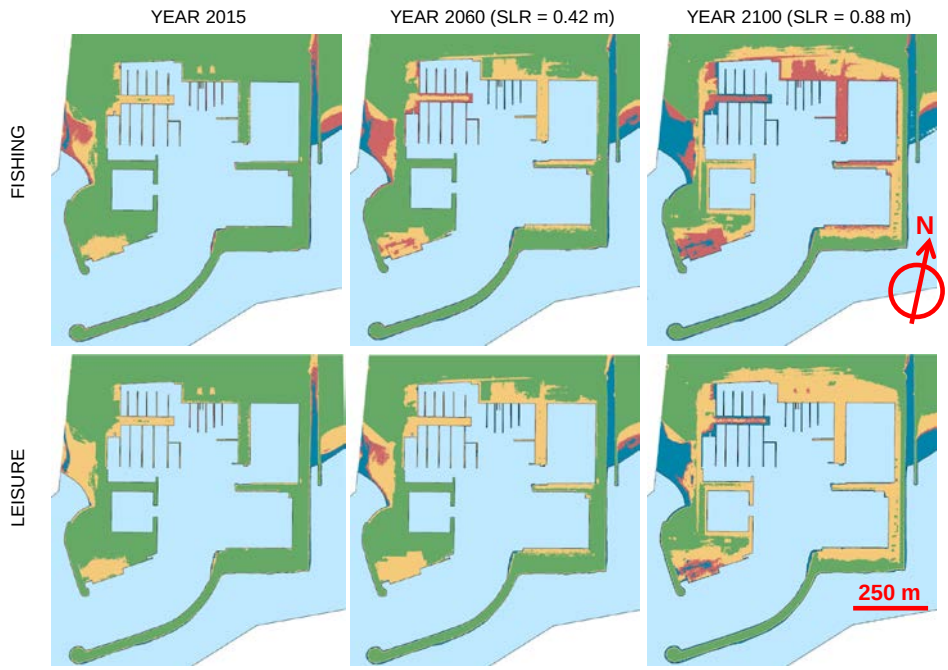

Figure 8. Operability maps of Vilanova I la Geltrú port in year 2015, 2060 and 2100 for the different port uses. Coloured areas indicate the port operability status: Maximum (green), minimum (light brown), not operable (red) and flooded (blue).

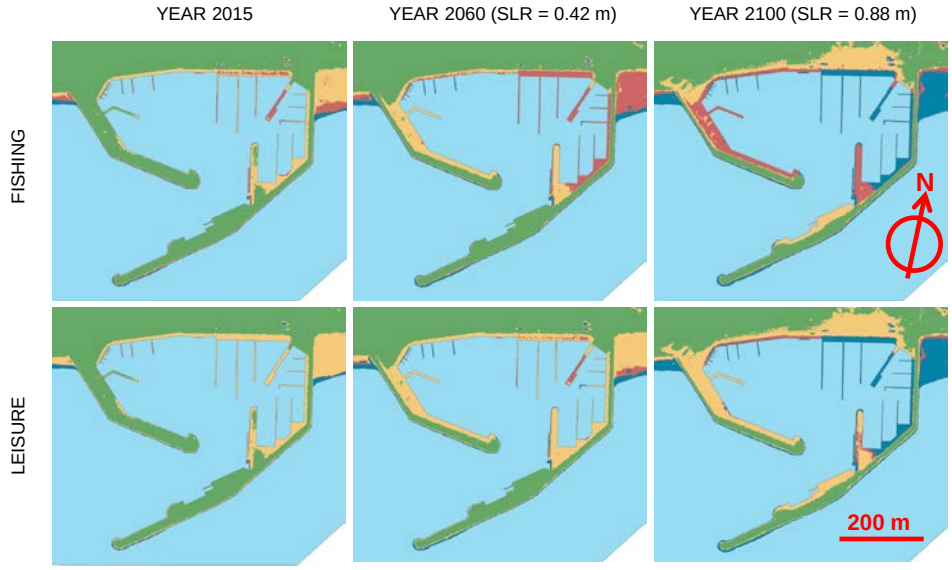

Figure 9. Operability maps of Cambrils port in year 2015, 2060 and 2100 for the different port uses. Coloured areas indicate the port operability status: Maximum (green), minimum (light brown), not operable (red) and flooded (blue).

4. DISCUSSION

4.1 About the methodology

The building of each port DEM required a quality control check of LAS points in order to remove spurious data typically associated to the presence of highly reflective structures such as glass windows of big buildings or metal roofs. This source of errors has been extensively reported in the literature (Bater and Coops, 2008), however in this study it represents less than the 1% of the total port surface.

Although the TINs are more complex than rasters and can easily accommodate different sampling densities, where rasters cannot, in this case study the DEM has been used as it is more efficient space wise than TINs. The accuracy and resolution of DEMs in coastal environments, where there

394 are relatively small differences in elevation over large areas, are of special interest. At low
395 elevations and gradients, the signal magnitude approaches the noise level of the measurements,
396 which can lead to large errors in inundation extent forecasts. This issue is particularly important for
397 developed coastal environments where the spatial extent of inundation can have disproportionate
398 consequences in terms of loss of life and property (Small and Sohn, 2015). Nevertheless, the
399 homogeneous and flat nature of docks and piers allows to use less dense grids (compared with
400 other geoscience areas) and simple interpolation methods to derive the DEM. Lloyd and Atkinson
401 (2012) conclude that sophisticated approaches do not significantly increase accuracy in the final
402 result.

403 The uncertainty in SLR projections is transmitted to the final port operability results. The RCP8.5
404 SLR values have been chosen in this study as the possible highest scenario and consequently the
405 obtained results represent an upper limit of port inoperability, according to IPCC projections.
406 Nevertheless, recent studies project much higher mean SLR for 2100: up to 1.86 m (Jevrejeva et
407 al., 2012; Mori et al., 2013) or even up to 2 m (Rahmstorf, 2007). This very extreme SLR is
408 physically feasible although with a very low probability of occurrence (<5 % by 2100, Jevrejeva et
409 al., 2014). Therefore, the increase of inoperability in the studied ports could even be worse,
410 reducing the response capacity of ports to adapt to these changes. On the contrary, SLR also
411 could be lower than that considered in the application carried out in this work, in particular if the
412 global mitigation measures proposed in the Paris Agreement are reached. In this case, the actual
413 SLR would be smaller, close to that projected in the RCP2.6 scenario from AR5 (IPCC, 2013).

414 Anyway, whatever the SLR, the proposed methodology is still valid and band confidence analysis
415 could be added to the final result by constructing different operability maps for different climate
416 change scenarios to plan well in advance the most suitable responses to such impacts. This is
417 necessary and of special importance, since the planning horizon in port engineering usually is of
418 20 or 25 years, due to the different phases that must be followed: diagnosis of the current situation,
419 forecast of maritime traffic evolution, assessment of infrastructure and superstructure needs, study
420 of alternatives including an economic-financial analysis for each of them, design of the selected

421 alternative including and analysis of its compatibility with urban planning, study of environmental
422 impact assessment, period of public information and discussion, tender and execution of the works
423 in several phases (each one lasting several years) to minimize the interference with port activity.

424 The proposed methodology has not considered the variability of the mean water level due to
425 meteorological effects such as those generated by atmospheric pressure or wind. The main
426 reasons to do that are: (i) daily meteorological oscillations can be considered negligible in the area
427 (EPPE, 2014) and extreme events, due to its nature, are considered as episodic processes that
428 rarely extend more than few hours (Mendoza, 2008) and (ii) According to Conte and Lionello
429 (2014) there is not statistical evidence that storm surge frequency and magnitude will change
430 significantly in future in the Mediterranean coast. However, storm surge oscillations should be
431 considered in areas with different meteorological conditions, where relevant storm surges are more
432 frequent and may last longer time spans, since this effect would significantly worsen port
433 operability conditions.

434 In the same way, other effects such as wave run-up or overtopping over the docks have not been
435 considered because such infrastructure is located in sheltered areas, where the wave effects are
436 limited and only may be significant in the case of very strong storms, which are episodic events.

437 The used approach considers the future port operability by taking the present port infrastructures
438 and operations as a reference. Port facilities will change in time due to the need of ports to
439 accommodate to new trade demands, maritime traffic features and vessel characteristics.
440 According to UNCTAD (2017) additional traffic resulting from economic growth can be expected
441 and improvements in ship technology, structure and materials will lead to even bigger megaships,
442 particularly within the container shipping industry. In the same way, Mangan (2017) does not
443 foresee any major “disruptive innovation” radically reshaping the shipping sector but observed
444 trends suggest the existence of a global shipping network serviced by mega-ships. He also points
445 out that disruptions to the maritime freight transport network can have rapid and wide-range effects
446 in economies and societies.

447 In addition, for the sake of simplicity, a stretch of dock or pier has been defined as inoperable when
448 the freeboard is smaller than the thresholds defined in table 3. Nevertheless, in some cases and
449 taking special precautions (e.g. loading or unloading very carefully or reducing velocity) operations
450 could be carried out even if the vessel was berthed in a structure with a freeboard in the range of
451 inoperability.

452 Therefore, the results obtained in this study have to be understood as potential impacts and the
453 values presented as indicative, but they can be useful for future port expansion plans. The
454 operability is quantified as a percentage with respect the total length of the analyzed use. The time
455 evolution of this indicator is a good descriptor of the global port operability in time but should not be
456 understood as a detailed descriptor of a specific infrastructure functioning. This is principally true
457 when considering the commercial use; in that case a reduction of 7% of the total activity can
458 represent an unacceptable inoperability of certain infrastructure (terminal or berthing area) due to
459 the economic and social impact generated by the unfeasibility of doing the operation for a certain
460 type of vessel (EPPE, 2000). This may lead to traffic deviations and, as a consequence, losses in
461 monetary and prestige terms for the port. This could cause malfunction to the entire port and for
462 this reason has to be considered as unacceptable. Therefore, in this case, port authorities should
463 act carrying out appropriate actions to prevent such level of inoperability (e.g. engineering works to
464 increase operability or adaptation of other port areas to give service to this type of traffic). Because
465 of this, the obtained values should be understood as a measure of the minimum degree of impact.

466 The present port snapshot showing the port operations and detailed type of infrastructures requires
467 an “on ground” survey because they are not necessarily reported in available memorandums. An
468 example of this is the existence of floating piers, that in some cases are described as piers but not
469 specifically as floating structures, which would not be affected by SLR.

470

471 **4.2 About the results**

The temporal evolution of inoperability for each port and for the analysed scenario is shown in Figure 10, assuming the simplifications described in the previous section (no adaptation measures and no changes in port morphology). There, dashed lines indicate a not operable status whereas solid lines represent the percentage of berths flooded (which are included in the percentage of inoperability).

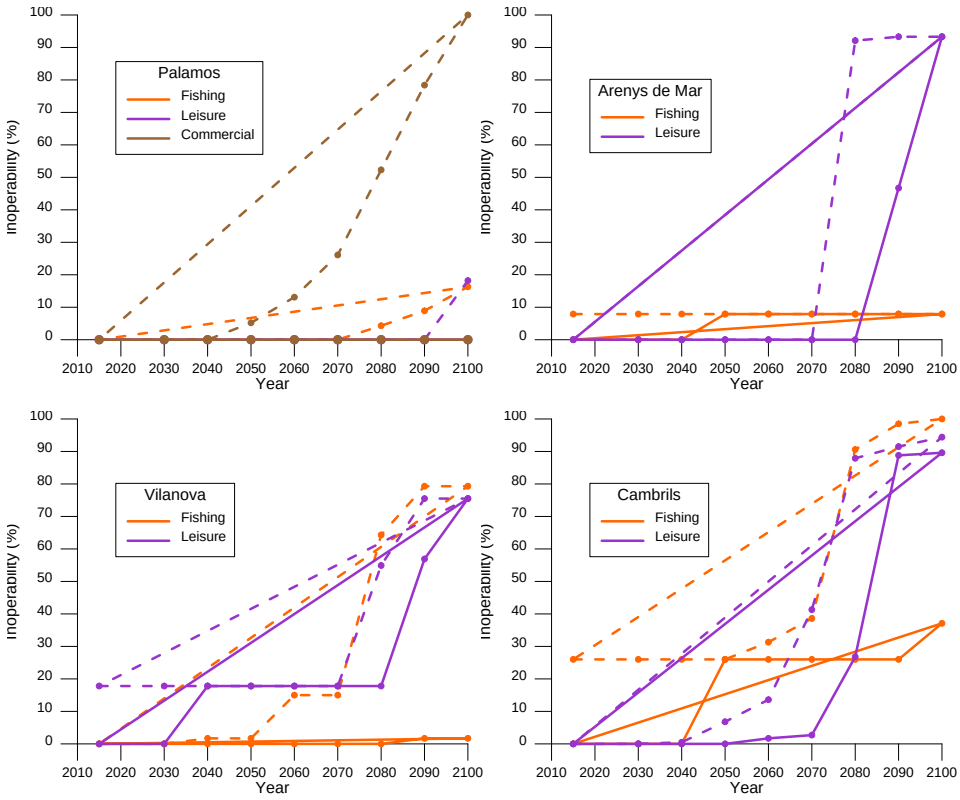

Figure 10. Evolution of the inoperability during the 21st century at the four studied ports. The colour refers to the port use. Dashed lines indicate inoperability. Solid lines indicate flooding.

The plots of Figure 10 show, in high detail, the evolution of the berthing inoperability during the studied period. The advantage of these graphics is that they allow to visualize abrupt changes in the percentage of inoperability or flooding. Such sudden changes are tipping points, which according to Kwadijk et al. (2010) may be understood as moments where the magnitude of change due to climate change or SLR is such that the current management strategy will no longer be able to meet the objectives and, therefore, other strategies are needed if the operability conditions want to be maintained. To the best knowledge of the authors the adaptation strategy for the studied ports is business as usual, i.e. the ports do not have specific master plans that accommodate their uses to future SLR. The identification of these tipping points allows port authorities to establish adaptation pathways, i.e. to define different strategies over time to cope with the negative impacts of SLR. Due to the necessary time for port planning, as indicated in the previous Section, the early knowledge of the possible impacts and potential adaptation strategies enables port authorities to allocate the necessary means for undertaking the appropriate measures to overcome the impacts.

According to Figure 10 in Palamós port no berths of any type are flooded throughout the century. In the case of leisure berths, the piers located within the inner basin and northwards from it appear in the maps as flooded (Figure 6). Nevertheless, these are floating piers with a very low freeboard. Due to their floating nature, they are not considered flooded, because they follow sea level oscillations, easily accommodating to higher levels and remaining operational all the time.

With respect to the commercial berths, they are fully operational until 2040, when the percentage of inoperability begins to increase reaching 26% in 2070. From that year, the percentage of inoperability grows at a faster rate, being 100% in 2100. On the contrary the fishing berths only are affected after 2070, when the inoperability percentage gently increases up to 16% in 2100. Meanwhile, the leisure berths are unaffected until 2090, but henceforth the inoperability grows until 18% in 2100. These results indicate that the fishing and leisure berths at Palamós port may face the SLR in the worst scenario (from IPCC-AR5) without requiring any adaptation measure until the last part of the century. On the contrary, under this scenario, the commercial berths would need

adaptation measures by the middle of the century. The tipping points in this port are 2040, 2070 and 2090 for the commercial, fishing and leisure functions respectively.

At Arenys de Mar, at present, the 8% of the fishing sector has a freeboard lesser than the recommended threshold (EPPE, 2012). This is because such zone is occupied by small fishing boats, which need a smaller freeboard. Only these berths with smaller freeboard are inoperative throughout the century, although from 2050 onwards they become flooded.

Concerning the leisure craft zone, all the docks and piers are fully operative for much of the century, but after 2070 there is a very fast increase of inoperability and in 2080 92% of this area is located under the threshold freeboard, slightly increasing to 93% in 2090 and 2100. In addition, after 2080 much of this sector becomes quickly flooded with a percentage of about 47% in 2090 and 93% in 2100.

In summary, a tipping point at year 2040 is identified for fishing activities, when some of the berths that are located below the threshold freeboard but operating for small boats will become flooded. Another tipping point is in 2070, when most of the leisure zone starts to be inoperative, being most of it flooded after 2080.

The commercial activity at Vilanova i la Geltrú has not been analysed in this study because it gives service to small general cargo vessels, which need very low freeboards (lower than those indicated in ROMS 2.0-11). Therefore, for this specific function and considering the minimum freeboard levels suggested in ROMS 2.0-11, all the commercial berths would be inoperative throughout the whole century. Therefore, the application of the followed methodology does not make sense for this type of docks, and for this reason their inoperability due to SLR has not been assessed.

The fishing berths are all operative until 2040, when 2% are located below the threshold freeboard. After 2050 there is an increase of the inoperability of such berths reaching 15% until 2070, when this inoperability abruptly rises reaching 79% in 2090 and 2100.

In the case of leisure crafts, 18% of the port berths are at present theoretically inoperative. As in previous cases this is because they are occupied by small boats, which practically do not need

freeboard. Nevertheless, since 2040 these berths will be flooded becoming totally inoperative. The percentage of berths dedicated to leisure crafts under the operability threshold sharply rises after 2070, reaching 55% in 2080 and 76% in 2100. The percentage of flooded berths follows a similar trend, but with a delay of 10 years.

Observing Figure 10 several tipping points can be observed in this port for each function. For the fishing crafts, such points are located in 2030 (when some berths start to be flooded) and in 2070 (when the percentage of inoperability triggers). In the case of leisure crafts, the tipping points are found in 2030 (some berths start to be inoperative), 2050 (the rate of inoperability becomes larger) and 2070 (when the inoperability sharply rises).

The last port analysed is Cambrils, where only fishing and leisure crafts are moored. As in the case of Arenys de Mar port and for the same reasons, part (26%) of the fishing docks are under the recommended operability threshold. This quantity remains unchanged until 2050, when it starts to slightly increase reaching 39% in 2070. After this year the inoperability of the fishing area experiences an abrupt change, being 91% in 2080 and 100% in 2100. On the other hand, the present 26% of docks under the operability threshold become flooded in 2050. This percentage of flooded berths remains unaltered until 2100, when it amounts to 32%.

In this port, the leisure craft berths are fully operative until 2040. Afterwards the inoperability increases until 14% in 2060, when it quickly rises, reaching 88% in 2080. From that moment, the reduction of operability is smoother, until 94% in 2100. Concerning the berthing area flooded, this is zero until 2050, slightly increasing after until 3% in 2070. After this year the flooded area quickly increases, reaching 89% in 2090 and 90% in 2100.

The tipping points in Cambrils for the fishing area are 2040 (when some docks start to be flooded), 2050 (when the number of inoperative berths increases) and 2070 (when there is a sharp increase of the inoperability). In the case of leisure crafts, the tipping points are located in 2040 (when some berths start to be inoperative) and 2060 (when the rate of inoperability quickly rises).

In summary, for the SLR scenario considered (RCP8.5 from IPCC), all the studied ports will experience, to a greater or lesser extent, reductions of their operability due to SLR and for all activities (fishing, leisure and eventually commercial). In the last part of the century, in particular after 2070, in most of the cases the reductions of operability will be very significant, generating disruptions of the service and large economic loses if no adaptation measures are taken.

5. CONCLUSIONS

In this paper, a methodological framework based on LiDAR-derived DEMs has been developed to assess the impact of SLR on port operability. The proposed approach considers the change of MWL (including tide and SLR) in time, the type of use of the port facility and its typology, allowing to determine its operability according to some predefined thresholds. This methodology has been applied to four ports considering the RCP8.5 scenario of the IPCC, showing to be useful to detect those berthing areas that for each service (commercial, leisure and fishery) will become inoperative and when this will occur.

Results show that, assuming the present port morphology and that scenario, which is the worst projected by IPCC, during the 21st century the operability of Catalan ports would decrease as a consequence of SLR and the subsequent reduction of the freeboard in berthing areas. The developed methodology could be applied for other scenarios, so that ports could have a wide range of possible impacts for planning well in advance the most suitable responses to such impacts. This is necessary and of special importance, since horizon planning in port engineering usually is of 20 or 25 years, due to the different phases that must be followed. Anyway, port authorities have the capability and the technical means to undertake the necessary adaptation measures to prevent potential negative impacts (whatever they are) generated by SLR.

In summary, this work shows that the developed methodology is a very useful tool for port authorities to detect potential impacts in port operability and, in particular, tipping points involving major changes in their efficiency. Therefore, it may contribute to help in the early design of the necessary adaptation pathways to overcome the expected impacts.

Acknowledgements

The work described in this publication was funded by the European Union's Seventh Framework Programme through the grant to the budget of the Collaborative Project RISES-AM-, Contract FP7-ENV-2013-two-stage-603396. The support of the Secretaria d'Universitats i Recerca del Departament d'Economia i Coneixement de la Generalitat de Catalunya (Ref 2017SGR773) is also acknowledged. Finally, the authors are also grateful to the Institut Cartogràfic i Geològic de Catalunya (ICGC) for providing the data used in this study.

6. REFERENCES

Addo, K. A., Walkden, M., & Mills, J. (2008). Detection, measurement and prediction of shoreline recession in Accra, Ghana. ISPRS Journal of Photogrammetry and Remote Sensing, 63, 543–558.

Alexander, C., Tansey, K., Kaduk, J., Holland, D., & Tate, N. J. (2010). Backscatter coefficient as an attribute for the classification of full-waveform airborne laser scanning data in urban areas. ISPRS Journal of Photogrammetry and Remote Sensing, 65, 423–432.

Bater, C. W., & Coops, N. C. (2008). Evaluating error associated with LiDAR-derived DEM interpolation. Computers & Geosciences, 35, 289–300.

Becker, A., Inoue, S., & Fischer, M. (2012). Climate change impacts on international seaports : knowledge , perceptions, and planning, efforts among port administrators. Climatic Change, 110, 5-29.

613 Behrenfeld, M. J., Hu, Y., O'Malley, R. T., Boss, E. S., Hostetler, C. A., Siegel, D. A., Sarmiento, J.
614 L., Schulien, J., Hair, J. W., & Lu, X. (2017). Annual boom-bust cycles of polar phytoplankton
615 biomass revealed by space-based LiDAR. Nature Geoscience, 10, 118–122.
616
617 Bolaños, R., Jordà, G., Cateura, J., Lopez, J., Puigdefabregas, J., Gomez, J., & Espino, M. (2009)
618 The XIOM: 20 years of a regional coastal observatory in the Spanish Catalan coast. Journal of
619 Marine Systems, 77, 237–260.
620
621 Brennan, R., & Webster, T. (2006). Object-oriented land cover classification of LiDAR derived
622 surfaces. Canadian Journal of Remote Sensing, 32, 162–172.
623
624 Brown, I. (2006). Modelling future landscape change on coastal floodplains using a rule-based
625 GIS. Environtal Modelling and Software, 21, 1479-1490.
626
627 Buffington, K. J., Dugger, B. D., Thorne, K- M., & Takekawa, J. Y. (2016). Statistical correction of
628 LiDAR-derived digital elevation models wuth multispectral airborne imagery in tidal marshes.
629 Remote Sensing of Environment, 186, 616-625.
630
631 Burcharth, H. F., Lykke Andersen, T., & Lara, J. L. (2014). Upgrade of coastal defence structures
632 against increased loadings caused by climate change: A first methodological approach.
633 Coastal Engineering, 87, 112-121.
634
635 Chehata, N., Guo, L., & Mallet, C. (2009). Airborne LiDAR feature selection for urban classification
636 using random forests. International Archives of the Photogrammetry, Remote Sensing and
637 Spatial Information Sciences, 39, 207–212.
638
639 Chini, N., & Stansby, P. K. (2012). Extreme values of coastal wave overtopping accounting for
640 climate change and sea level rise. Coastal Engineering, 65, 27-37.

Chu-Agor, M. L., Muñoz-Carpena, R., Kiker, G., Emanuelsson, A., & LInkoz, I. (2011). Exploring vulnerability of coastal habitats to sea level rise through global sensitivity and uncertainty analyses. Environtal Modelling and Software, 26, 593-604.

Clough, J., Polaczyk, A., & Propato, M. (2016). Modeling the potential effects of sea-level rise on the coast of New York: Integrating mechanistic accretion and stochastic uncertainty. Environtal Modelling and Software, 84, 349-362.

Collin, A., Archambault, P., & Long, B. (2008). Mapping the shallow water seabed habitat with the SHOALS. IEEE Transactions on Geoscience and Remote Sensing, 46, 2947–2955.

Collister, B. L., Zimmerman, R. C., Sukenik, C. I., Hill, V. J., & Balch, W. M. (2018). Remote sensing of optical characteristics and particle distributions of the upper ocean using shipboard LiDAR. Remote Sensing of Environment, 215, 85-96.

Conte, D., & Lionello, P. (2014). Storm surge distribution along the Mediterranean coast: Characteristics and evolution. Procedia - Social and Behavioral Sciences, 120, 110-115.

Cooper, H. M., Chen, Q., Fletcher, C. H., & Barbee, M. M. (2013). Assessing vulnerability due to sea-level rise in Maui, Hawai'I using LiDAR remote sensing GIS. Climatic Change, 116, 547-563.

Costa, B. M., Battista, T. A., & Pittman, S. J. (2009). Comparative evaluation of airborne LiDAR and ship-based multibeam SoNAR bathymetry and intensity for mapping coral reef ecosystems. Remote Sensing of Environment, 112, 1082-1100.

DPTOP (2007). Pla de Ports de Catalunya. Departament de Política Territorial i Obres Públiques. Generalitat de Catalunya, Barcelona, Spain.

EPPE (2000). ROM 3.1-99. Design of the maritime configuration of ports, approach channels and harbour basins. Recommendations for maritime works Series 3, Puertos del Estado, Ministerio de Fomento, Madrid, Spain.

EPPE (2012). ROM 0.2-11. Recomendaciones para el proyecto y ejecución en obras de ataque y amarre. Puertos del Estado, Ministerio de Fomento, Madrid, Spain.

EPPE (2014). REDMAR. RED de Mareógrafos de Puertos del Estado. [online: http://calipso.puertos.es/BD/informes/globales/GLOB_2_3_3758.pdf].

Gesch, D. B. (2009). Analysis of LiDAR elevation data for improved identification and delineation of lands vulnerable to sea-level rise. Journal of Coastal Research, 25, 49–58.

Goulden, T., Hopkinson, C., Jamieson, R., & Sterling, S. (2014). Sensitivity of watershed attributes to spatial resolution and interpolation method of LiDAR DEMs in three distinct landscapes. Water Resources Research, 50, 1908–1927.

Goulden, T., Hopkinson, C., Jamieson, R., & Sterling, S. (2016). Sensitivity of DEM, slope, aspect and watershed attributes to LiDAR measurement uncertainty. Remote Sensing of Environment, 179, 23-35.

Guo, L., Chehata, N., Mallet, C., & Boukir, S. (2011). Relevance of airborne LiDAR and multispectral image data for urban scene classification using random forests. ISPRS Journal of Photogrammetry and Remote Sensing, 66, 56–66.

Con formato: Español (España)

Código de campo cambiado

696 Hallegatte, S., Ranger, N., Mestre, O., Dumas, P., Corfee-Morlot, J., Herweijer, C., & Wood, R. M.
697 (2011). Assessing climate change impacts, sea level rise and storm surge risk in port cities: a
698 case study on Copenhagen. Climatic Change, 104, 113–137.
699
700 Hill, V., Matrai, P., Olson, E., Suttles, S., Steele, M., Codispoti, L., & Zimmerman, R. (2013).
701 Synthesis of integrated primary production in the Arctic Ocean: II. In situ and remotely sensed
702 estimates. Progress in Oceanography, 110, 107–125.
703
704 Hladik, C., & Alber, M. (2012). Accuracy assessment and correction of a LIDAR-derived salt marsh
705 digital elevation model. Remote Sensing of Environment, 121, 224-235.
706
707 IPCC (2013). Climate change 2013. The physical science basis. In: Stocker, T. F., Qin, D.,
708 Plattner, G. -K., Tignor, M., Allen, S. K., Boschung, J., Nauels, A., Xia, Y., Bex, V., & Midgley,
709 P. M. (eds.). Cambridge University Press, Cambridge, United Kingdom and New York, NY,
710 USA, 1535.
711
712 Isobe, M. (2013). Impact of global warming on coastal structures in shallow water. Ocean
713 Engineering, 71, 51–57.
714
715 Jevrejeva, S., Grinsted, A., Moore, J. C. (2014). Upper limit for sea level projections by 2100.
716 Environmental Research Letters 9, 104008.
717
718 Jevrejeva, S., Moore, J. C., Grinsted, A. (2012). Sea level projections to AD2500 with a new
719 generation of climate change scenarios. Global Planetary Change, 80–81, 14–20.
720
721 Kane, H. H., Fletcher, C. H., Frazer, L. N., & Barbee, M. M. (2015). Critical elevation levels for
722 flooding due to sea-level rise in Hawaii. Regional Environmental Change, 15, 1679-1687.
723

724 Knapp, N., Fischer, R., & Huth, A. (2018). Linking LiDAR and forest modeling to assess biomass
725 estimation across scales and disturbance states. Remote Sensing of Environment, 205, 199-
726 209.
727
728 Kwadijk, J. C. J., Haasnoot, M., Mulder, J. P. M., Hoogvliet, M. M. C., Jeuken, A. B. M., van der
729 Krogt, R. A. A., van Oostrom, N. G. C., Schelfhout, H. A., van Velzen, E. H., van Waveren, H.,
730 & de Wit, M. J. M. (2010). Using adaptation tipping points to prepare for climate change and
731 sea level rise: a case study in the Netherlands. WIREs Climate Change, 1, 729-740.
732
733 Le Cozannet, G., Rohmer, J., Cazenave, A., Idier, D., van de Wal, R., de Winter, R., Pedreros, R.,
734 Balouin, Y., Vinchon, C., & Oliveros, C. (2015). Evaluating uncertainties of future marine
735 flooding occurrence as sea-level rises. Environtal Modelling and Software, 73, 44-56.
736
737 Lloyd, C. D., & Atkinson, P. M., 2002. Deriving DSMs from LiDAR data with kriging. International
738 Journal of Remote Sensing, 23, 2519–2524.
739
740 Mangan, J. (2017). Future of the sea: Trends in the transport of goods by sea. Foresight,
741 Government Office for Science, London, UK, 23 p.
742
743 Mase, H., Tsujio, D., Yasuda, T., & Mori, N. (2013). Stability analysis of composite breakwater with
744 wave-dissipating blocks considering increase in sea levels, surges and waves due to climate
745 change. Ocean Engineering, 71, 58-65.
746
747 Mendoza, E. T. (2008). Coastal vulnerability to storms in the Catalan coast. PhD thesis, Universitat
748 Politecnica de Catalunya, Barcelona, Spain.
749
750 Monioudi, I. N., Karditsa, A., Chatzipavlis, A., Alexandrakis, G., Andreadis, O. P., Velegrakis, A. F.,
751 Poulos, S. E., Ghionis, G., Petrakis, S., Sifnioti, D., Hasiotis, T., Lipakis, M., Kampanis, N.,

752 Karambas, T., & Marinos, E. (2016). Assessment of vulnerability of the eastern Cretan
753 beaches (Greece) to sea level rise. Regional Environmental Change, 16, 1952-1962.
754
755 Mori, N., Shimura, T., Yasuda, T., Mase, H. (2013). Multi-model climate projections of ocean
756 surface variables under different climate scenarios: future change of waves, sea level and
757 wind. Ocean Engineering, 71, 122–129.
758
759 Ng, A. K. Y., Chen, S. -L., Cahoon, S., Brooks, B., & Yang, Z. (2013). Climate change and the
760 adaptation strategies of ports: The Australian experiences. Research in Transportation
761 Business & Management, 8, 186-194.
762
763 Nicholls, R. J., Marinova, N., Lowe, J. A., Brown, S., Gusmão, D., Hinkel, J., & Tol, R. S. J. (2011).
764 Sea-level rise and its possible impacts given a 'beyond 4ºC world' in the twenty-first century.
765 Philosophical Transactions of the Royal Society A, 369, 161–181.
766
767 Paudel, Y., Botzen, W. J. W., & Aerts, J. C. J. H. (2015). Influence of climate change and socio-
768 economic development on catastrophe insurance: a case study of flood risk scenarios in the
769 Netherlands. Regional Environmental Change, 15, 1717-1729.
770
771 Pe'eri, S., & Long, B. (2011). LiDAR technology applied in coastal studies and management.
772 Journal of Coastal Research, 62, 1–5.
773
774 Poulter, B., & Halpin, P. N. (2008). Raster modelling of coastal flooding from sea-level rise.
775 International Journal of Geographical Information Science, 22, 167-182.
776
777 Rahmstorf, S. (2007). A semi-empirical approach to projecting future sea-level rise. Science 315,
778 368-370.
779

780 Revell, D. L., Battalio, R., Spear, B., Ruggiero, P., & Vandever, J. (2011). A methodology for
781 predicting future coastal hazards due to sea level rise on the California Coast. Climatic
782 Change, 109, 251-276.
783
784 Revell, D., Komar, P., & Sallenger, A. (2002). An application of LiDAR to analyses of El Niño
785 erosion in the Netarts Littoral Cell, Oregon. Journal of Coastal Research, 18, 792–801.
786
787 Richter, A., Faust, D., & Maas, H. G. (2013). Dune cliff erosion and beach width change at the
788 northern and southern spits of Sylt detected with multi-temporal LiDAR. Catena, 103, 103–111.
789
790 Sánchez-Arcilla, A., Mösso, C., Sierra, J. P., Mestres, M., Harzallah, A., Senouci, M., & Raey, M.
791 E. (2011). Climatic drivers of potential hazards in Mediterranean coasts. Regional
792 Environmental Change, 11, 617-636.
793
794 Sánchez-Arcilla, A., Sierra, J. P., Brown, S., Casas-Prat, M., Nicholls, R. J., Lionello, P., & Conte,
795 D. (2016). A review of potential physical impacts on harbours in the Mediterranean Sea under
796 climate change. Regional Environmental Change, 16, 2471-2484
797
798 Shrestha, R., Carter, W., Sartori, M., Luzum, B., & Slatton, K. (2005). Airborne laser swath
799 mapping: Quantifying changes in sandy beaches over time scales of weeks to years. ISPRS
800 Journal of Photogrammetry and Remote Sensing, 59, 222–232.
801
802 Sierra, J. P., Casanovas, I., Mösso, C., Mestres, M., & Sánchez-Arcilla, A. (2016). Vulnerability of
803 Catalan (NW Mediterranean) ports to wave overtopping due to different scenarios of sea level
804 rise. Regional Environmental Change, 16, 1457-1468.
805
806 Sierra, J. P., & Casas-Prat, M. (2014). Analysis of potential impacts on coastal areas due to
807 changes in wave conditions. Climatic Change, 124, 861–876.

Con formato: Español (España)

Con formato: Español (España)

Sierra, J. P., Garcia-León, M., Gracia, V., & Sánchez-Arcilla, A. (2017b). Green measures for Mediterranean harbours under a changing climate. Proceedings of the Institution of Civil Engineers – Maritime Engineering, 170, 55-66.

Sierra, J. P., Genius, A., Lionello, P., Mestres, M., Mösso, C., & Marzo, L. (2017a). Modelling the impact of climate change on harbour operability: The Barcelona port case study. Ocean Engineering, 141, 64-78.

Small, C., & Sohn, R. (2015). Correlation scales of digital elevation models in developed coastal environments. Remote Sensing of Environment, 159, 80-85.

Stive, M. J. F. (2004). How important is global warming for coastal erosion? Climatic Change, 64, 27-39.

Stockdon, H. F., Doran, K. S., & Sallenger, A. H. (2009). Extraction of LiDAR-based dune-crest elevations for use in examining the vulnerability of beaches to inundation during hurricanes. Journal of Coastal Research, 25, 59–65.

Straatsma, M. W., & Middelkoop, H. (2006). Airborne laser scanning as a tool for lowland floodplain vegetation monitoring. Hydrobiologia, 565, 87−103.

Suh, K. -D., Kim, S. -W., Kim, S., & Cheon, S. (2013). Effects of climate change on stability of caisson breakwaters in different water depths. Ocean Engineering, 71, 103-112

Torresan, S., Critto, A., Rizzi, J., & Marcomini, A. (2012). Assessment of coastal vulnerability to climate change hazards at the regional scale: the case study of the North Adriatic Sea. Natural Hazards and Earth System Sciences, 12, 2347–2368.

836
837 UNCTAD (2017). Review of maritime transport 2018. United Nations Conference on Trade and
838 Development, Geneva, Switzerland, 116 p.
839
840 Vousdoukas, M. I., Mentaschi, L., Voukouvalas, E., Verlaan, M., Jevrekeva, S., Jackson, L. P.,
841 Feyen, L. (2018). Global probabilistic projections of extreme sea levels show intensification of
842 coastal flood hazard. Nature Communications, 9, 2360, doi: 10.1038/s41467-018-04692-w.
843
844 Webster, T. L., Forbes, D. L., MacKinnon, E., & Roberts, D. (2006). Flood-risk mapping for storm-
845 surge events and sea-level rise using LiDAR for southeast New Brunswick. Canadian Journal
846 of Remote Sensing, 32, 194–211.
847
848 White, S., & Wang, Y. (2003). Utilizing DEMs derived from LiDAR data to analyze morphologic
849 change in the North Carolina coastline. Remote Sensing of Environment, 85, 39–47.
850
851 Wu, S. -Y., Najjar, R., & Siewert, J. (2009). Potential impacts of sea-level rise on the Mid- and
852 Upper-Atlantic region of the United States. Climatic Change, 95, 121-138.
853
854 Wulder, M. A., White, J. C., Nelson, R. F., Næsset, E., Ørka, H. O., Coops, N. C., Hilker, T., Bater,
855 C. W., & Gobakken, T. (2012). LiDAR sampling for large-area forest characterization: a review.
856 Remote Sensing of Environment, 121, 196–209.
857
858 Yamamoto, K. H., Powell, R. L., Anderson S., & Sutton, P. C. (2012). Using LiDAR to quantify
859 topographic and bathymetric details for sea turtle nesting beaches in Florida. Remote Sensing
860 of Environment, 125, 125-133.
861 Yin, J., Griffies, S.M., Stouffer, R.J. (2010). Spatial variability of sea level rise in twenty-first century
862 projections. Journal of Climate, 23, 4585-4607.
863

Zawada, D. G., & Brock, J. C. (2009). A multiscale analysis of coral reef topographic complexity using LiDAR-derived bathymetry. Journal of Coastal Research, 25, 6–15.

Zhang, K. (2011). Analysis of non-linear inundation from sea-level rise using LiDAR data: a case study for South Florida. Climatic Change 106, 537-565.

Zhou, W. (2013). An object-based approach for urban land cover classification: Integrating LiDAR height and intensity data. IEEE Geoscience and Remote Sensing Letters, 10, 928–931.

877 FIGURE CAPTIONS

878 Figure 1. Flowchart of the construction of a DEM of a port. Area of Interest refers to a polygon created
879 reflecting a specific port extension, its port use, the type of infrastructure and the water body.

880 Figure 2. Data sets, TIN and DEM obtained for the harbour of Cambrils (Catalonia, Spain).

881 Figure 3. Upper, mean and lower limit of SLR projection for the Mediterranean Sea under the RCP8.5
882 scenario.

883 Figure 4. Port operability categories.

884 Figure 5. Location of the 4 studied ports and view of their layouts. P: Palamós, A: Arenys de Mar, V:
885 Vilanova i la Geltrú, C: Cambrils. Graphical scales have been added to give an idea of their dimensions.
886 Coloured areas indicate port use: commercial (dark brown), leisure (purple) and fishing (orange). Non-
887 coloured areas correspond to other uses (e.g. dry docks) not analysed.

888 Figure 6. Operability maps of Palamós port in year 2015, 2060 and 2100 for the different port uses. Coloured
889 areas indicate the port operability status: Maximum (green), minimum (light brown), not operable (red) and
890 flooded (blue).

891 Figure 7. Operability maps of Arenys de Mar port in year 2015, 2060 and 2100 for the different port uses.
892 Coloured areas indicate the port operability status: Maximum (green), minimum (light brown), not operable
893 (red) and flooded (blue).

894 Figure 8. Operability maps of Vilanova I la Geltrú port in year 2015, 2060 and 2100 for the different port
895 uses. Coloured areas indicate the port operability status: Maximum (green), minimum (light brown), not
896 operable (red) and flooded (blue).

897 Figure 9. Operability maps of Cambrils port in year 2015, 2060 and 2100 for the different port uses. Coloured
898 areas indicate the port operability status: Maximum (green), minimum (light brown), not operable (red) and
899 flooded (blue).

900 Figure 10. Evolution of the inoperability during the 21st century at the four studied ports. The colour refers to
901 the port use. Dashed lines indicate inoperability. Solid lines indicate flooding.